DOI: 10.1002/((please add manuscript number))
Article type: Communication

L-DOPA coated manganese oxide nanoparticles as dual MRI contrast agents and drug delivery vehicles

Birgitte Hjelmeland McDonagh, Gurvinder Singh, Sjoerd Hak, Sulalit Bandyopadhyay, Ingrid Lovise Augestad*, *Davide Peddis*, *Ioanna Sandvig*, *Axel Sandvig, and Wilhelm Robert Glomm*

Birgitte Hjelmeland McDonagh, Sulalit Bandyopadhyay, Dr. Wilhelm Robert Glomm
Uglestad Laboratory, Department of Chemical Engineering, Norwegian University of Science and Technology, 7491, Norway
E-mail: birgitte.h.mcdonagh@ntnu.no
Dr. Gurvinder Singh,
Department of Materials Science and Engineering, Norwegian University of Science and Technology, 7491, Norway
Dr. Sjoerd Hak,
Department of Circulation and Medical Imaging, Norwegian University of Science and Technology, 7491, Norway
Ingrid Lovise Augestad, Dr. Ioanna Sandvig, Dr. MD. Axel Sandvig
Department of Neuroscience, Norwegian University of Science and Technology, 7491, Norway
Dr. Davide Peddis,
Institute of Structure and Matter, National Research Council, Monterotondo Scalo, Italy
Dr. Ioanna Sandvig
John Van Geest Centre for Brain Repair, Department of Clinical Neurosciences, University of Cambridge, CB2 OPY Cambridge, UK
Dr. MD. Axel Sandvig
Division of Pharmacology and Clinical Neurosciences, Department of Neurosurgery, Umeå University, 901 87, Sweden
Dr. Wilhelm Robert Glomm
Sector for Biotechnology and Nanomedicine, SINTEF Materials and Chemistry, 7465, Norway

Keywords: Manganese, Contrast Agents, MRI, L-DOPA

Imaging soft tissue of the human body with magnetic resonance imaging (MRI) is sometimes crucial for determining an accurate diagnosis. Acquired images can reveal obstructed blood flow, abnormal tissue structure and vascularization. To improve the accuracy of diagnosis, the contrast can be altered by administering magnetically active contrast agents (CAs), typically comprised of chelated ions such as gadolinium (Gd^{3+}) and manganese (Mn^{2+}). CAs can either enhance or decrease the contrast in the tissue depending on their magnetic

susceptibilities, and CAs are referred to as either *positive* or *negative*, respectively. With the upsurge in synthesis and characterization of magnetically active nanoparticles (NPs), new nanoparticle-based systems with potential applications towards theranostics are emerging. NPs have longer blood circulation times as compared to chelates, [1] and the large surface-to-volume ratio of NPs results in a greater contact area between magnetically active centers and the tissue. Moreover, the large surface area of NPs can be modified with biologically compatible molecules and drugs, which allows for simultaneous diagnostics and therapy. Positive *T1* CAs are generally preferred because they give a hyperintense signal that is easier to distinguish from surrounding tissue and less likely to be confused with artefacts. *T1* CAs are typically prepared from paramagnetic elements, such as Gd^{3+} and Mn^{2+}, as they effectively shorten the local spin-lattice relaxation time (*T1*) in the tissue. While chelates of gadolinium are used in the clinics (*e.g* Gadovist, Magnevist),[1,2] they suffer from challenges such as short circulation times, and severe side effects in patients with poor kidney function. [3, 4] Novel *T1* CAs must address these issues and simultaneously give equal or better contrast. Mn^{2+} ions are Ca^{2+} analogues and can enter neurons through voltage-gated Ca^{2+} ion channels, [5] which enables *in vivo* neuronal tract tracing in Manganese Enhanced MRI (MEMRI). [6, 7] Administrating high concentrations of Mn^{2+} ions can affect the *T2*/*T2** times as well, [8,9] however, high doses of Mn^{2+} can accumulate in the brain and cause a toxic condition named *manganism*. [10] Because of the toxicity, manganese-chelates are still regarded as alternative CAs in MRI. However, recent synthesis of manganese oxide-based NPs could lead to a resurgence of manganese as an MRI contrast agent, [11-14] and a recent report by Zhang et al demonstrate the efficacy of Mn^{2+} ions as imaging probes for visualizing delivery of cancer therapeutic drugs. [15] Also, manganese oxide NPs (MONPs) are *T2* active CAs, but they also degrade in water within a reasonable time-frame (hours to days). [12, 16-18] This is interesting for MR applications because MONPs that degrade, release Mn^{2+} ions, which are very efficient *T1*

CAs. [19-22] MONPs therefore offer a time-dependent *T1* and *T2*/*T2** contrast switch that allows complementary MR images and improved diagnostics.

Generally, metal oxide NPs are surface functionalized to be stable in water, by attaching either a stabilizing ligand, or a functional molecule which not only imparts colloidal stability but also additional diagnostic/therapeutic function to the NP. The neurotransmitter dopamine is frequently used as a surface anchor connecting the surface oxide layer of the metal oxide NP with an outer polymer shell. [23-25] The hallmark of Parkinson's disease (PD) is gradual degeneration of dopaminergic neurons in the *Substantia Nigra pars compacta* (SNpc), leading to deficient dopamine content and severe cognitive and motor deficits. Dopamine is an important neurotransmitter for the function of the human retina and optic nerve (ON) [26, 27] and visual impairments in PD are common. [28] The symptoms can be caused by deficient dopamine content, [28] or from fiber layer thinning of the optic nerve. [29,30] Although dopamine is biologically relevant, the properties of its precursor, *L*-3,4-dihydroxyphenylalanine (L-DOPA), are far more interesting. L-DOPA is carried across the BBB *via* the LAT1 transporter, and is decarboxylated to dopamine in capillary endothelial cells. [31, 32] L-DOPA is orally administered and currently the drug of choice for patients suffering from Parkinson's disease (PD).

While L-DOPA functionalized MONPs can act as a scaffold for attachment to other functional molecules,[33] L-DOPA used both as a stabilizer and active drug has not been reported previously.

The objectives of this study were as follows: First, we wanted to characterize how fast and in what way the MONPs degrade in water. Second, we wanted to determine the magnetic properties of MONPs, and whether release of Mn^{2+} from MONPs is efficient enough to gain complementary images *in vivo*. Finally, we wanted to determine whether L-DOPA is released from the NPs, which may be of value for potential applications in Parkinson's disease (PD).

Experimental Section

Synthesis and characterization of MONPs.

In a typical synthetic procedure, MONPs (15±5 nm) were synthesized *via* thermal decomposition of Mn-oleate in a high boiling point organic solvent (Figure 1a). [34, 35] High resolution transmission electron microscopy (HRTEM) suggests a core-shell morphology of Mn_2O_3-MnO NPs (Figure 1b). The lattice fringe spacing of the core (~2.49 Å) corresponds to the separation between the (211) lattice planes of tetragonal Mn_3O_4. The lattice spacing of the shell (~2.2 Å) corresponds well to (200) interplanar spacing of MnO. The MnO shell has an average thickness of ~2.1 nm. The X-ray diffraction (XRD) pattern also suggests the presence of mixture of phases in MONPs (Figure S2).[36] The investigation of magnetic properties confirms the morpho-structural characterization, suggesting the presence of Mn_3O_4-MnO phases. Bulk Mn_3O_4 is a ferrimagnetic spinel-type compound (Curie temperature, $T_{C,Mn2O3}$=43 K), while MnO is an antiferromagnetic compound (Néel temperature, $T_{N,\ MnO}$=100 K). [36] Temperature dependence of magnetization measuring in Field Cooling (FC) condition shows a transition around 40 K (close to T_C of Mn_3O_4) suggesting that the magnetic behavior of the sample is dominated by the ferrimagnetic Mn_3O_4 (Figure S3). This is supported by the field dependence of magnetization, showing a quasi-static behavior at 5 K and paramagnetic behavior at 80 K (above T_C). It is important to underline that the hysteresis loop at 5 K shows a clear non-saturating character at high field, suggesting the presence of an antiferromagnetic contribution that can be ascribed to the presence of a small quantity of MnO in the shell. [36-38] In addition, X-ray photoelectron spectroscopy (XPS) showed mixed oxidation states of MONPs (Figure S4-6), that further support the HRTEM, XRD and magnetic measurements described above.

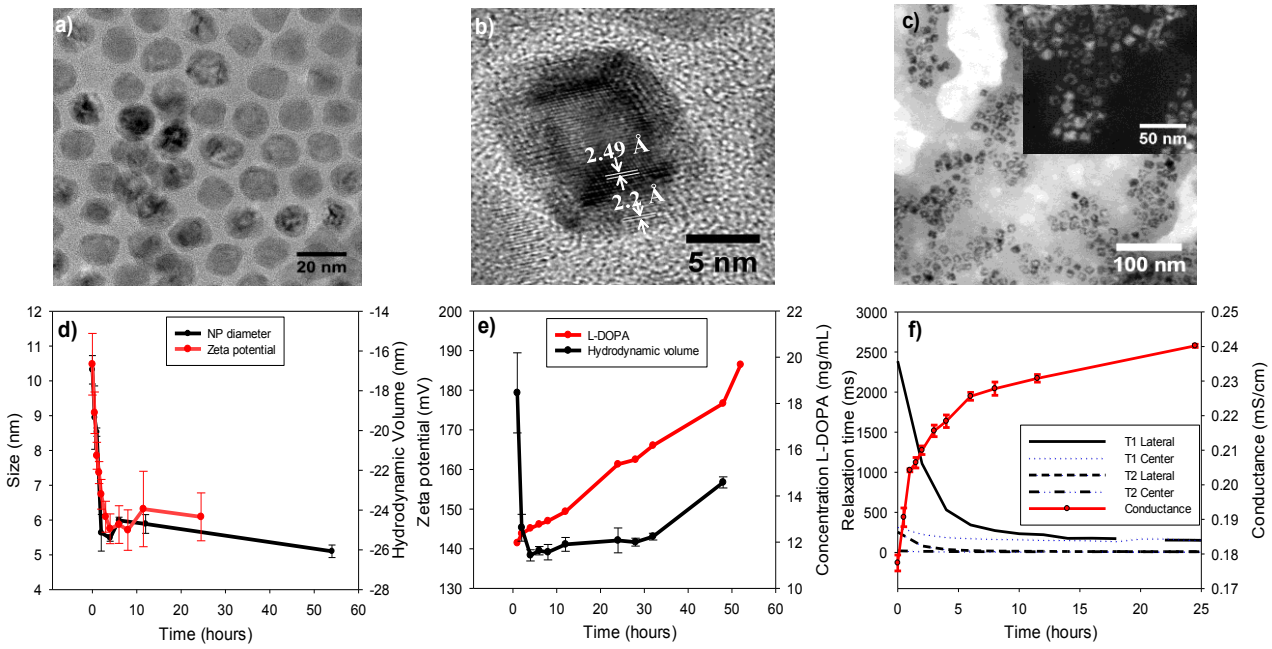

Figure 1: MONPs degrade in water and release L-DOPA. a) TEM of MONPs in organic phase **b)** HRTEM image of MONPs before surface modification **c)** TEM of L-DOPA coated MONPs, 1 hour in water (pH=6.8). Inset shows dark field image of hollow MONPs after 1 hour in water **d)** Size and ζ-potential of MONPs as a function of time **e)** Hydrodynamic volume and concentration of L-DOPA as a function of time **f)** *T1* and *T2* relaxation time in pig eyes upon injection of MONPs, as a function of time. "Lateral" refers to the opposite side of the injection site, while "Center" refers to the mid part of the pig eye. Conductance as a function of time is also shown.

A simple one-step protocol was used to functionalize the MONPs with L-DOPA and transfer the NPs from organic to water phase.[39] After functionalization, MONPs were collected with centrifugation and dispersed in MilliQ water (5mg/mL). Earlier studies have shown that when anchoring dopamine on metallic NPs, the two hydroxyl groups in the aromatic ring bind to the oxide layer of the NP surface, and the amine group is oriented towards the bulk.[23-25] At the pH used here (pH=6.8), the carboxylic acid moiety of L-DOPA is deprotonated, and functionalized MONPs were found to be negatively charged (Figure 1d). As L-DOPA only differs from dopamine by a carboxylic group, the surface organization of L-

DOPA is most likely identical to that of dopamine, *i.e.*; with its carboxylic group pointing outwards. From XPS measurements, MONPs surface functionalized with L-DOPA showed the presence of nitrogen, which was absent prior to functionalization (Figure S.5). Also, high resolution C1 spectra showed contribution of C-O, C-N, C-C and O-C=O, which combined with the N-peak suggests that the L-DOPA molecules are anchored to MONPs *via* its two hydroxyl groups. Thus, bulk-oriented carboxylic acid groups can act as anchor points for addition of secondary molecules onto NPs by covalent bonding with amine groups, *e.g. via* carbodiimide chemistry.

After one hour in water, the average MONP diameter is halved (Figure 1d). TEM images reveal that MONPs are no longer dense particles, but smaller structures with a quadratic edge and a hollow interior (Figure 1c). This indicates that MONPs degrade via oxidation and dissolve in water, releasing Mn^{2+}. [20] Oxidation of NPs that leads to hollow or porous structures is caused by the Kirkendall effect, which describes that atomic diffusion is caused by an exchange of vacancies, and not by an interchange of atoms. [40] Here, the outward diffusion of Mn^{2+} ions is exchanged with an inward flux of vacancies. With time, the manganese oxide shell breaks and the fragments continue to degrade until they are completely dissolved (Figure S1).

Even though NPs disintegrate in water, they still appear to cluster together (Figure 1c). The hydrodynamic volume (V_H) is orders of magnitudes larger than the diameter estimated from TEM images (Figure 1e), which indicates that the NPs form clusters. The value of the ζ potential increases with time (Figure 2a), which could be due to changes in adlayer concentration, reorientation, or change in the surface affinity of L-DOPA.

Functional molecules are usually attached to NPs with a covalent bond, and a successful drug delivery vehicle must not only carry the drug, but also release it. Breaking the covalent bond *in vivo* can be a challenge, and may impair drug delivery efficiency. Since MONPs disintegrate in water, L-DOPA will eventually be released form the MONPs. The

bulk concentration of L-DOPA steadily increases with decreasing NP diameter (Figure 1e). Our results show that the MONPs disintegrate in water within 50 hours, releasing L-DOPA into the surrounding medium.

In order to assess their use as CAs in biological systems, the time-dependent contrast switch of MONPs was described in pig eyes, *ex vivo*. Pig eyes are similar to human eyes, the specimen size allows for a good signal-to-noise ratio, and they offer a more biologically relevant matrix compared to agarose gels, which are more widely used.[41] MONPs coated with L-DOPA were freshly prepared, injected into pig eyes, and scanned with MRI over a period of 35 hours.

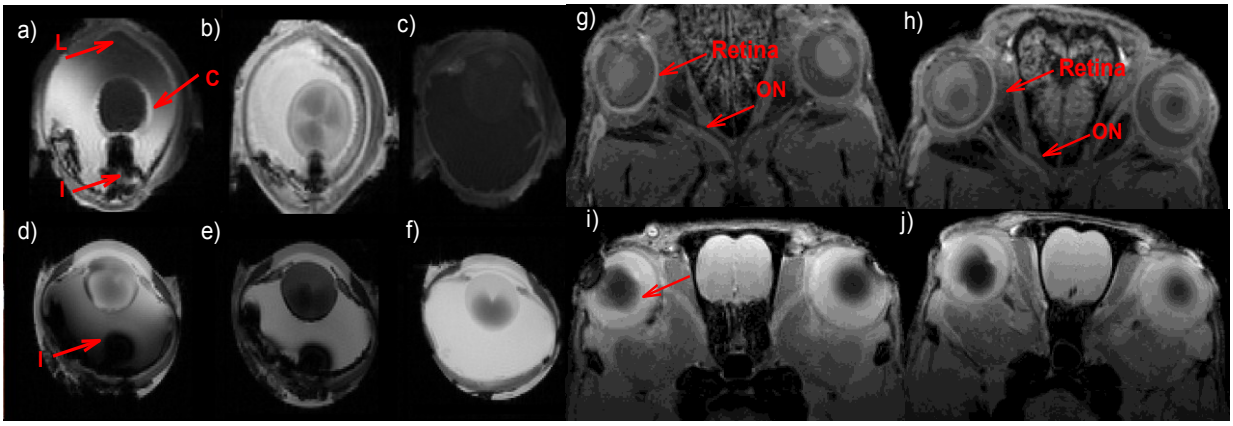

Figure 2: *Ex vivo* and *in vivo* degradation of MONPs. Images **a)** and **b)** show the *T1w* images of a pig eye injected with MONPs, acquired immediately after injection and after 34 hours, respectively. "L" refers to the lateral side of the injection site "I", while "C" refers to the central part of the pig eye. Images **d)** and **e)** show the *T2*w* images. **c)** *T1w* and **f)** *T2*w* image of the control eye. **g)** *T1w* and **i)** *T2*w* image of rat ON and retina, 1 hour post injection

Release of Mn^{2+} is clearly visible in the *T1*w image, as it takes the form of a bright hyperintense cloud surrounding the hypointense injection site (Figure 2a). In the *T2**w image, the Mn^{2+} ions and MONPs give rise to negative contrast as well, proving the dual properties of manganese as active *T1* and *T2** CAs (Figure 2d). [19]

With time, the negative contrast decreases in both the *T1w* (Figure 2b) and *T2*w* (Figure 2e) images, while the positive contrast in the *T1w* image completely fills the whole intravitreal space (Figure 2b). The *T1* and *T2* relaxation times in the pig eyes rapidly decrease after injection of MONPs. In particular, the *T1* relaxation time at the center of the eye decreases with a simultaneous increase in the conductance (Figure 1f). A change in the conductance indicates a change in the ionic strength of the suspension. [42] The change in conductance and the concomitant effect on relaxation times and *ex vivo* contrast, suggests that MONPs disintegrate into Mn^{2+}.

The rodent visual system is an established model for investigating damage and repair in the central nervous system (CNS), [43, 44] as it is easily accessible and immune privileged.[45, 46] Enhanced visualization of the ON tract can be achieved by administering contrast agents into the vitreous body. The contrast in the rat retina is significantly enhanced compared to the contralateral control eye immediately upon injection of MONPs (Figure 2g). The *T2** contrast (Figure 2i, j) is not clearly separated from the rodent lens, but after 24 hours, the contrast moves towards the retina. This movement is also seen in the complementary *T1w* images (Figure 2 h). With time, the contrast in the ON increases as well (Figure 2h). MONPs are likely too large to be taken up by the retinal ganglion cells, but Mn^{2+} ions can.[9, 44] We have previously used $MnCl_2$ to study optic nerve regeneration in several animal models. [9, 44, 47] However, using MONPs opens up for complementary and long term imaging without injecting additional doses of CAs.

In conclusion, we have developed MONPs functionalized with L-DOPA that gradually degrade in biological media, releasing Mn^{2+} ions and L-DOPA. As CAs in MRI, MONPs give negative contrast, but as they disintegrate in water, a concomitant release of Mn^{2+} ions gives a positive contrast. The system described here, thus offers a time-dependent switch in the MR contrast from dark to bright, which allows for complementary imaging and enhanced

diagnosis. While further studies are needed to determine the effect of L-DOPA coated MONPs in a PD model, we have herein described a system that can release L-DOPA and that has potential as a drug delivery vehicle.

Acknowledgements: The Department of Chemical Engineering, NTNU, is acknowledged for financial support. The Research Council of Norway is acknowledged for the support to the Norwegian Micro- and Nano-Fabrication Facility, NorFab (197411/V30).

Received: ((will be filled in by the editorial staff))
Revised: ((will be filled in by the editorial staff))
Published online: ((will be filled in by the editorial staff))

1. Xu, W.; Kattel, K.; Park, J. Y.; Chang, Y.; Kim, T. J.; Lee, G. H. *PCCP* **2012,** 14, (37), 12687-12700.
2. Westbrook, C., Kaut Roth, C., Talbot, J., *MRI in Practice*. 4 ed.; Blackwell Publishing Ltd: USA, 2011.
3. Kuo, P. H.; Kanal, E.; Abu-Alfa, A. K.; Cowper, S. E. *Radiology* **2007,** 242, (3), 647-649.
4. Penfield, J. G.; Reilly, R. F. *Nat Clin Pract Neph* **2007,** 3, (12), 654-668.
5. Silva, A. C.; Bock, N. A. *Schizophr. Bull.* **2008,** 34, (4), 595-604.
6. Aoki, I.; Wu, Y.-J. L.; Silva, A. C.; Lynch, R. M.; Koretsky, A. P. *NeuroImage* **2004,** 22, (3), 1046-1059.
7. Olsen, Ø.; Kristoffersen, A.; Thuen, M.; Sandvig, A.; Brekken, C.; Haraldseth, O.; Goa, P. E. *J. Magn. Reson. Imaging* **2010,** 32, (3), 551-560.
8. Thuen, M.; Berry, M.; Pedersen, T. B.; Goa, P. E.; Summerfield, M.; Haraldseth, O.; Sandvig, A.; Brekken, C. *J. Magn. Reson. Imaging* **2008,** 28, (4), 855-865.
9. Mørch, Ý. A.; Sandvig, I.; Olsen, Ø.; Donati, I.; Thuen, M.; Skjåk-Bræk, G.; Haraldseth, O.; Brekken, C. *Contrast Media Mol. Imaging* **2012,** 7, (2), 265-275.
10. Fitsanakis, V. A.; Zhang, N.; Avison, M. J.; Gore, J. C.; Aschner, J. L.; Aschner, M. *Neurotoxicology* **2006,** 27, (5), 798-806.
11. Zhen, Z.; Xie, J. *Theranostics* **2012,** 2, (1), 45-54.
12. Chen, Y.; Yin, Q.; Ji, X.; Zhang, S.; Chen, H.; Zheng, Y.; Sun, Y.; Qu, H.; Wang, Z.; Li, Y.; Wang, X.; Zhang, K.; Zhang, L.; Shi, J. *Biomaterials* **2012,** 33, (29), 7126-7137.
13. Kueny-Stotz, M.; Garofalo, A.; Felder-Flesch, D. *Eur. J. Inorg. Chem.* **2012**, (12), 1987-2005.
14. Choi, E. S.; Park, J. Y.; Baek, M. J.; Xu, W.; Kattel, K.; Kim, J. H.; Lee, J. J.; Chang, Y.; Kim, T. J.; Bae, J. E.; Chae, K. S.; Suh, K. J.; Lee, G. H. *Eur. J. Inorg. Chem.* **2010**, (28), 4555-4560.
15. Zhang, L.; Zhang, Z.; Mason, R. P.; Sarkaria, J. N.; Zhao, D. *Sci. Rep.* **2015,** 5, 9874.
16. Lim, E. K.; Kim, T.; Paik, S.; Haam, S.; Huh, Y. M.; Lee, K. *Chem. Rev.* **2015,** 115, (1), 327-394.
17. Xing, R.; Zhang, F.; Xie, J.; Aronova, M.; Zhang, G.; Guo, N.; Huang, X.; Sun, X.; Liu, G.; Bryant, L. H.; Bhirde, A.; Liang, A.; Hou, Y.; Leapman, R. D.; Sun, S.; Chen, X. *Nanoscale* **2011,** 3, (12), 4943-4945.

18. Kim, T.; Momin, E.; Choi, J.; Yuan, K.; Zaidi, H.; Kim, J.; Park, M.; Lee, N.; McMahon, M. T.; Quinones-Hinojosa, A.; Bulte, J. W. M.; Hyeon, T.; Gilad, A. A. *J. Am. Chem. Soc.* **2011,** 133, (9), 2955-2961.
19. Shapiro, E. M.; Koretsky, A. P. *Magn. Reson. Med.* **2008,** 60, (2), 265-269.
20. Shin, J.; Anisur, R. M.; Ko, M. K.; Im, G. H.; Lee, J. H.; Lee, I. S. *Angewandte Chemie - International Edition* **2009,** 48, (2), 321-324.
21. Berkowitz, A. E.; Rodriguez, G. F.; Hong, J. I.; An, K.; Hyeon, T.; Agarwal, N.; Smith, D. J.; Fullerton, E. E. *Physical Review B - Condensed Matter and Materials Physics* **2008,** 77, (2).
22. Salazar-Alvarez, G.; Sort, J.; Suriñach, S.; Baró, M. D.; Nogués, J. *J. Am. Chem. Soc.* **2007,** 129, (29), 9102-9108.
23. Patel, D.; Kell, A.; Simard, B.; Xiang, B.; Lin, H. Y.; Tian, G. *Biomaterials* **2011,** 32, (4), 1167-1176.
24. Xu, C.; Xu, K.; Gu, H.; Zheng, R.; Liu, H.; Zhang, X.; Guo, Z.; Xu, B. *J. Am. Chem. Soc.* **2004,** 126, (32), 9938-9939.
25. Huang, J.; Xie, J.; Chen, K.; Bu, L.; Lee, S.; Cheng, Z.; Li, X.; Chen, X. *Chem. Commun.* **2010,** 46, (36), 6684-6686.
26. Reis, R. A. M.; Ventura, A. L. M.; Kubrusly, R. C. C.; de Mello, M. C. F.; de Mello, F. G. *Brain Res. Rev.* **2007,** 54, (1), 181-188.
27. Kubrusly, R. C. C.; Guimarães, M. Z. P.; Vieira, A. P. B.; Hokoç, J. N.; Casarini, D. E.; De Mello, M. C. F.; De Mello, F. G. *J. Neurochem.* **2003,** 86, (1), 45-54.
28. Harnois, C.; Di Paolo, T. *Invest. Ophthalmol. Vis. Sci.* **1990,** 31, (11), 2473-2475.
29. Inzelberg, R.; Ramirez, J. A.; Nisipeanu, P.; Ophir, A. *Vision Res.* **2004,** 44, (24), 2793-2797.
30. Archibald, N. K.; Clarke, M. P.; Mosimann, U. P.; Burn, D. J. *Brain* **2009,** 132, (5), 1128-1145.
31. Pardridge, W. M. *NeuroRx* **2005,** 2, (1), 3-14.
32. Laterra J, K. R., Betz LA, et al., *Blood-Brain Barrier. In: Siegel GJ, Agranoff BW, Albers RW, et al., editors. Basic Neurochemistry: Molecular, Cellular and Medical Aspects*. 6 ed.; Lippincott-Raven, Available from: http://www.ncbi.nlm.nih.gov/books/NBK28180/: Philadelphia, 1999.
33. Bae, K. H.; Lee, K.; Kim, C.; Park, T. G. *Biomaterials* **2011,** 32, (1), 176-184.
34. Schladt, T. D.; Graf, T.; Tremel, W. *Chem. Mater.* **2009,** 21, (14), 3183-3190.
35. Chen, W.; Lu, F.; Chen, C. C. V.; Mo, K. C.; Hung, Y.; Guo, Z. X.; Lin, C. H.; Lin, M. H.; Lin, Y. H.; Chang, C.; Mou, C. Y. *NMR Biomed.* **2013,** 26, (9), 1176-1185.
36. Si, P. Z.; Li, D.; Choi, C. J.; Li, Y. B.; Geng, D. Y.; Zhang, Z. D. *Solid State Commun.* **2007,** 142, (12), 723-726.
37. Si, P. Z.; Li, D.; Lee, J. W.; Choi, C. J.; Zhang, Z. D.; Geng, D. Y.; Brück, E. *Appl. Phys. Lett.* **2005,** 87, (13), 1-3.
38. Belviso, C.; Agostinelli, E.; Belviso, S.; Cavalcante, F.; Pascucci, S.; Peddis, D.; Varvaro, G.; Fiore, S. *Microporous Mesoporous Mater.* **2015,** 202, (C), 208-216.
39. Xie, J.; Chen, K.; Huang, J.; Lee, S.; Wang, J.; Gao, J.; Li, X.; Chen, X. *Biomaterials* **2010,** 31, (11), 3016-3022.
40. Yin, Y.; Rioux, R. M.; Erdonmez, C. K.; Hughes, S.; Somorjal, G. A.; Alivisatos, A. P. *Science* **2004,** 304, (5671), 711-714.
41. Guduric-Fuchs, J.; Ringland, L. J.; Gu, P.; Dellett, M.; Archer, D. B.; Cogliati, T. *Mol. Vis.* **2009,** 15, 1915-1928.
42. Atkins, P. W.; De Paula, J., *Atkins' physical chemistry*. Oxford University Press: Oxford, 2014; p XXV, 1008 s. : ill.

43. Sandvig, I.; Thuen, M.; Hoang, L.; Olsen, Ø.; Sardella, T. C. P.; Brekken, C.; Tvedt, K. E.; Barnett, S. C.; Haraldseth, O.; Berry, M.; Sandvig, A. *NMR Biomed.* **2012,** 25, (4), 620-631.
44. Sandvig, A.; Sandvig, I.; Berry, M.; Olsen, Ø.; Pedersen, T. B.; Brekken, C.; Thuen, M. *J. Magn. Reson. Imaging* **2011,** 34, (3), 670-675.
45. Zhou, R.; Caspi, R. R. *F1000 Biol. Rep.* **2010,** 2, (1).
46. Cramer, A. O.; MacLaren, R. E. *Curr. Gene Ther.* **2013,** 13, (2), 139-151.
47. Thuen, M.; Singstad, T. E.; Pedersen, T. B.; Haraldseth, O.; Berry, M.; Sandvig, A.; Brekken, C. *J. Magn. Reson. Imaging* **2005,** 22, (4), 492-500.